Research Square

Preprints are preliminary reports that have not undergone peer review.
They should not be considered conclusive, used to inform clinical practice,
or referenced by the media as validated information.

Learning and Coordinated Dispatch of Fusion Power Plants and Energy Storage With Delayed Tritium Circulation

Tan Peng
Shanghai Dianji University
Pengfei Zhao
Chinese Academy of Sciences
Dong Zhang
Shanghai Dianji University
Da Xie
xieda@sjtu.edu.cn

Shanghai Jiao Tong University
Mohannad Alhazmi
King Saud University

Research Article

Keywords: Fusion power, tritium fuel cycle, energy storage, constrained learning, Bayesian estimation, model predictive control

Posted Date: November 26th, 2026

DOI: https://doi.org/10.21203/rs.3.rs-11723507/v1

License: This work is licensed under a Creative Commons Attribution 4.0 International License.
Read Full License

Additional Declarations: No competing interests reported.

Learning and Coordinated Dispatch of Fusion Power Plants and Energy Storage With Delayed Tritium Circulation

Tan Peng[a], Pengfei Zhao[b], Dong Zhang[a], Da Xie[c,d,*], Mohannad Alhazmi[e]

[a] School of Intelligent Manufacturing and Robotics, Shanghai Dianji University, Shanghai 201306, China

[b] State Key Laboratory of Management and Control for Complex Systems, Institute of Automation, Chinese Academy of Sciences, Beijing 100864, China

[c] Department of Electrical Engineering, Shanghai Jiao Tong University, Shanghai 200240, China

[d] School of Electrical Engineering, Shanghai Dianji University, Shanghai 200240, China

[e] Electrical Engineering Department, College of Applied Engineering, King Saud University, P.O. Box 2454, 11451 Riyadh, Saudi Arabia

* Corresponding author. Email: xieda@sjtu.edu.cn (Da Xie).

Acknowledgments

The authors would like to acknowledge the support provided by Ongoing Research Funding Program, (ORF-2027-635), King Saud University, Riyadh, Saudi Arabia.

ABSTRACT

Tritium circulation couples fusion power delivery to the timing of fuel recovery. Material inside recycling and breeding equipment contributes to total inventory but remains unavailable for immediate withdrawal. This paper develops a mass-conserving compartment model and connects joint state–parameter estimation to thermal storage, battery operation, and extended dispatch. The formulation retains causal withdrawals, auxiliary consumption, conversion losses, and compartment-specific terminal resources. A prefix bound establishes the role of return timing in fuel availability. In an exact example, equal total inventories of 0.50 kg support different withdrawal sequences: only the earlier-return state supplies consecutive 0.15 kg requests. An energy bound then relates usable fuel to the support available from precharged storage. A 72 h numerical benchmark combines protected command-driven simulations with synthetic uncertainty and sensitivity calculations. The simulations separate rejected fuel requests from realized reserve violations and show how storage allocation changes delivery loss. The synthetic forecast experiment also quantifies the difference between marginal and complete-path coverage. These results identify fuel maturity, storage discharge limits, and temporal uncertainty as distinct constraints on dependable delivery. The resulting formulation links each electricity commitment to the material and energy available before that commitment falls due.

Keywords: Fusion power; tritium fuel cycle; energy storage; constrained learning; Bayesian estimation; model predictive control

1. INTRODUCTION

Fusion power plant design links dependable electricity delivery with the physical resources needed to sustain production. Net output depends on both installed thermal capacity and internal consumption. Heating, pumping, and fuel processing consume electricity before power reaches the grid. Studies of fusion in future electricity systems therefore distinguish reactor operation from net generation and account for flexibility [1], [2]. Fuel supply studies identify a separate constraint: tritium resources must support the deployment and operation of successive plants [3], [4]. Within a plant, each electricity commitment depends on fuel available before its associated withdrawal.

Most tritium supplied to a deuterium–tritium plasma can leave without reacting. This material returns through processing equipment. Newly bred tritium follows a separate extraction route. Both routes contain material that is present but temporarily unavailable. Dynamic fuel cycle studies connect circulation time, fueling efficiency, retention, and plant availability to inventory requirements [5], [6]. An adequate breeding ratio alone does not guarantee that fuel arrives before a scheduled withdrawal.

The timing constraint creates feedback between production and future availability. Increasing present output raises immediate withdrawal and changes later recycling and breeding inflows. A constraint based only on total stock omits this relationship. It can approve an electricity commitment whose supporting fuel remains inside a processing route. Equal starting inventories can therefore support different schedules when their internal distributions differ.

Energy storage changes the consequences of a temporary fuel gap. Thermal storage sustains turbine input while fusion heat decreases. A battery supports electricity delivery and auxiliary loads directly. Their usefulness depends on discharge power, stored energy, conversion losses, and subsequent recovery. Initial energy and terminal conditions are part of the comparison because an apparent operating benefit can arise from borrowing against the final inventory.

The internal fuel distribution is also uncertain. Flow measurements reveal only part of the state, while delayed inventory readings describe an earlier condition. Constant operation can hide residence parameters that become important during a disturbance. The framework estimates hidden inventories and process parameters jointly, then passes complete fuel trajectories to an extended dispatch problem.

The analysis establishes that equal usable and total starting stocks can support different near-term delivery schedules. The causal fuel bound identifies this difference, while the energy bound quantifies the resources available to bridge it. The numerical benchmark examines the same coupling through controlled dispatch trajectories and defined sensitivity experiments. Section 2 reviews related work and introduces the method schematic. Sections 3–5 develop the physical model, learning procedure, and dispatch analysis. Section 6 specifies the benchmark data and parameters. Section 7 presents the numerical results, followed by the conclusion in Section 8.

Table 1 Nomenclature

Symbol	Definition	Unit	Symbol	Definition	Unit
$t, k; \Delta t$	Interval, prediction step; interval length	h	$j \in \{r, b\}$	Recycling and breeding routes	–
s, N_p	Scenario or particle index; particle count	–	H, L, N	Delivery, extension, and total horizons	steps
f_t, b_t	Supplied and reacted tritium flow	kg/h	β, B	Effective burn fraction; breeding ratio	–
$v_{j,t}$	Input to fuel route j	kg/h	$q_{j,t}$	Return from route j	kg/h
m_t, M_t	Usable and total tracked tritium	kg	$x_{j,t}$	Internal compartment inventories	kg
A_j, c_j	Retained transfer matrix; return fractions	–	h_j, ℓ_j	Input allocation; loss fractions	–
λ, d_T	Decay rate; interval survival fraction	1/h; –	ℓ_a, e_t	Usable stock loss fraction; external supply	–; kg/h
$a_{j,l}$	Return kernel at lag l	–	$m_{res}, \overline{m}$	Usable reserve and capacity	kg
$\overline{f}, \overline{q}_j$	Feed and return flow capacities	kg/h	L_t	Total nondecay tritium loss rate	kg/h
Q_t, Q_t^h	Fusion heat and recovered useful heat	MW_{th}	κ	Reaction energy per tritium mass	MWh_{th}/ kg
y_t, v_t^+, v_t^-	Production, start, and stop indicators	–	$U, D; R^+, R^-$	Minimum dwell periods; heat ramp rates	steps; MW_{th}/h
H_t^g, H_t^c, H_t^d	Turbine heat, thermal charge, discharge	MW_{th}	H_t^w, E_t^H	Rejected heat; stored thermal energy	MW_{th}; MWh_{th}
P_t^g, P_t^a, P_t	Gross, auxiliary, and net electric power	MW	P_t^c, P_t^d, E_t^B	Battery charge, discharge, stored energy	MW; MWh
z_t^H, z_t^B	Storage charge mode indicators	–	η_h, η_g	Heat recovery and turbine efficiencies	–
η_c^H, η_d^H	Thermal charge and discharge efficiencies	–	η_c^B, η_d^B	Battery charge and discharge efficiencies	–
σ_H, σ_B	Interval energy retention fractions	–	P_0, P_y, E_{st}	Fixed and production auxiliaries; start energy	MW; MWh
χ_Q, χ_f, χ_r	Auxiliary conversion coefficients	see text	$D_t, \delta_t^-, \delta_t^+$	Delivery target, shortfall, and excess	MW
$\overline{I}, \overline{P}$	Import and export limits	MW	$c_Q, c_{st}, c_B, c_-, c_+$	Operating and deviation cost coefficients	see text
X_t, z_t	Physical state; estimator augmented state	mixed	θ, w_t	Process parameters; process uncertainty	mixed
o_t, d_t, ϵ_t	Measurements, bias, and measurement noise	mixed	δ_o, R_o	Observation delay; noise covariance	steps; mixed
D_t, π_t	Available observations; joint posterior	–	$\omega_t^{(s)}, J_k, G$	Particle weight; sensitivity; information matrix	mixed
$\underline{m}_{k\vee t}, \alpha_k$	Predictive lower bound; marginal risk	kg; –	$\varepsilon, \alpha, \gamma$	Fuel risk, CVaR level, confidence error	–
$u_k, u_k^{(s)}$	Common and scenario control vectors	mixed	C_s, L_s, ζ, ξ_s	Cost, shortage energy, and CVaR variables	$; MWh
ρ, C_W	Shortage risk price; conditional delivery capacity	$/MWh; MW	n_v, k_v, p_U	Validation episodes, failures, upper risk bound	–
$\overline{M}, \underline{Q}, \overline{Q}$	Total stock capacity; fusion heat bounds	kg; MW_{th}	p_r, p_b	Recycling and breeding transfer fractions	–
W, Ξ, F	Capacity window, scenario set, feasible trajectories	steps; –	$F_A, F_B, R_0^i(n)$	Feasible withdrawals; initial-stock returns	–; kg
$\lambda_\theta, \lambda_m, \theta_0$	Fitting weights and reference parameters	mixed	T_{tr}, V_{tr}	Training indices and prediction pairs	–
ξ, σ_m	Free fitting variables; inventory noise scale	mixed; kg	w_s, g_k	Scenario probability; fuel constraint margin	–; kg
X^{ref}, y^{ref}	Terminal physical and production references	mixed	r_t^M, r_t^E	Independent mass and energy-balance residuals	kg; power

2. Literature Review

2.1 Fuel cycle dynamics and inventory availability

Fusion fuel requirements arise within a broader plant design process. Federici et al. [7] describe the staged European DEMO design approach. Day et al. [8] address its tritium, matter injection, and vacuum systems, while Giegerich and Day [9] examine continuous vacuum pumping. These studies motivate an operational model with distinct routes and finite processing rates. Sawan and Abdou [10] establish conditions for fuel self-sufficiency, and Abdou et al. [5] relate those conditions to interacting physics and technology limits. Their long-run balance conditions provide necessary context for a short-run availability constraint.

Meschini et al. [6] develop dynamic fuel models for ARC- and STEP-class concepts. Their later analysis of trapping [11] distinguishes material retained in components from material immediately available for reuse. Slower transport, temporary retention, and loss can each reduce return flow. Distinguishing them depends on observation duration and channel availability.

TMAP8 supports transport and fuel cycle modeling [12], including a documented compartment benchmark [13]. FESTIM resolves hydrogen transport within components [14]. The recent workflow of Delaporte-Mathurin et al. (2026, unpublished preprint, arXiv:2603.25751) connects residence models with component physics. These tools resolve material transport under specified operating conditions. The dispatch formulation adds a decision layer in which operating choices generate the fuel trajectories that constrain later choices.

2.2 Fusion operation and storage coordination

Fusion system studies account for the value of operating flexibility [1], while unit commitment models represent mode-dependent operation [2]. UKAEA's Power Balance Models separate gross generation from auxiliary consumption [15]. This separation is retained here because storage may supply auxiliary loads even when reactor heat decreases.

Thermal storage technologies have different temperature ranges, losses, and integration requirements [16]. System-level storage value also depends on the relationship between duration and power capacity [17]. Trosino et al. [18] study the use of nuclear heat and thermal storage to supply flexible electricity. For batteries, Xu et al. [19] incorporate cycle aging into market operation. The present benchmark uses a simpler throughput charge. Its additional coupling is the alignment of thermal and electrical discharge with uncertain tritium recovery, while retaining common initial and terminal resources.

2.3 Learning and scheduling under uncertainty

Scientific structure can restrict data-driven models to physically meaningful behavior [20], [21]. Recursive identification also depends on the information contained in the input history [22]. Constrained estimation [23] and particle filtering [24], [25] provide complementary tools for hidden-state inference. Particle methods represent joint state and parameter uncertainty through weighted samples [26]. This paper uses these ideas to retain uncertainty over residence parameters and internal stocks rather than fitting usable inventory alone.

Learning-based predictive control connects estimation to repeated constrained decisions [27]. Stochastic MPC addresses forecast uncertainty [28]; robust optimization offers a different tradeoff between uncertainty protection and conservatism [29]. Scenario approaches give guarantees under stated sampling and decision assumptions [30], [31]. For nonconvex decisions, scenario guarantees depend on the adopted sampling and solution procedure [32]. The present formulation expresses feasibility relative to its retained scenarios and evaluates episode-level events separately.

Terminal restrictions influence the properties of predictive control [33], [34]. Predictive safety filters further illustrate how an action can be screened against future constraints [35]. The fuel guard enforces immediate withdrawal availability. The terminal extension separately constrains the resources remaining after delivery. Table 2 places these material and energy constraints within the established research streams.

A temporary interruption in fuel processing makes the scheduling distinction explicit. Eventual fuel recovery and sufficient aggregate energy leave the timing of withdrawals and turbine supply unresolved. The coupled model therefore retains the arrival time of usable fuel and the discharge time of stored energy. The associated learning task concerns uncertainty in the timing and quantity of recoverable fuel. That uncertainty enters dispatch through causal withdrawal constraints and the storage energy needed during recovery.

Table 2 Relationship between established methods and the dispatch problem

Research stream	Established capability	Retained decision boundary	Additional coupling here
Dynamic fuel cycles [5], [6], [11]	Circulation, breeding, and retention analysis	Fixed process design and mass accounting	Timely fuel for an electricity commitment
Fusion operation [1], [2]	Electrical value and operating states	Net power and equipment limits	Fuel returns driven by operating history
Energy storage [19], [20]	Energy transfer and operating costs	Separate thermal and battery balances	Discharge aligned with uncertain fuel recovery
Constrained learning and MPC [24], [28], [29]	Physical estimation and repeated decisions	Causal information and control	Joint uncertainty in residence and hidden stock

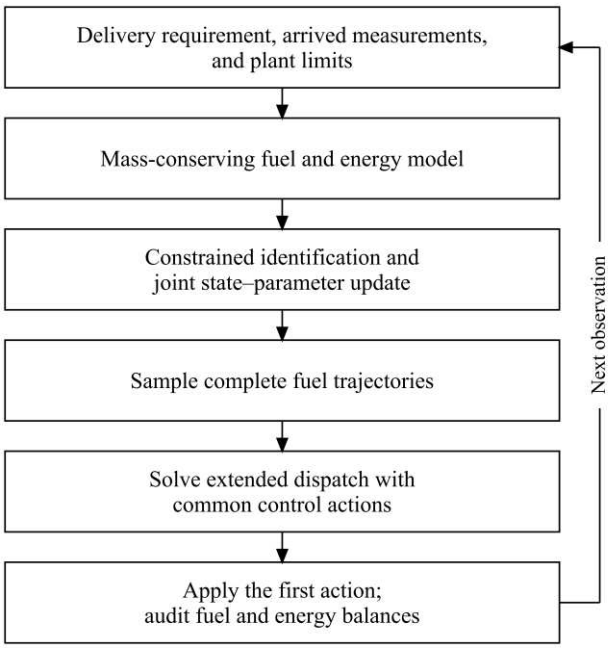

Fig. 1 Schematic of fuel-aware learning and coordinated storage dispatch

Fig. 1 connects the material balance to the electrical commitment through a repeated estimation and dispatch sequence. The current information set contains the delivery requirement, equipment limits, and measurements that have arrived. The joint update assigns usable stock, route inventories, and residence parameters to a common physical state. Sampled trajectories carry their dependence into the scheduling constraints, so each withdrawal changes the returns available later. Thermal storage and the battery enter through separate balances because they support delivery at different points in the conversion chain. Common control actions preserve the observation boundary across scenarios. The extended horizon then constrains the fuel distribution and stored energy remaining after the delivery window. Applying the first action closes one physical transition, after which the next measurements update the state. The balance audit checks that this transition preserves the declared material and energy accounts.

3. Fuel and Energy Conservation Model

3.1 System boundary and reaction consumption

Time advances in intervals of length Δt. All masses refer to tritium, and flows are interval averages. Usable storage connects to recycling and breeding routes, indexed by r and b. Deuterium is nonbinding. Fixed plant parameters define the operating envelope. Effective burn fraction, fusion heat, and route inflows satisfy

$$b_t = \beta f_t, 0 < \beta < 1. \tag{1}$$

$$Q_t = \kappa b_t. \tag{2}$$

$$v_{r,t} = f_t - b_t, v_{b,t} = B b_t. \tag{3}$$

The effective fraction includes fueling efficiency within the stated system boundary. Recycling returns unburned throughput, while breeding supplies new material. Immediate usable-stock depletion therefore scales with feed rather than burn.

3.2 Positive compartment dynamics

Route inventory $x_{j,t}$ is nonnegative. With survival factor $d_T = exp(-\lambda \Delta t)$, returns and retained stocks obey

$$q_{j,t} = \frac{d_T}{\Delta t} c_{j,t}^T x_{j,t}. \tag{4}$$

$$x_{j,t+1} = d_T A_{j,t} x_{j,t} + \Delta t h_j v_{j,t}. \tag{5}$$

Conservative transitions satisfy

$$\begin{gathered} 1^T A_{j,t} + c_{j,t}^T + \ell_{j,t}^T = 1^T, 1^T h_j = 1, \\ A_{j,t}, c_{j,t}, \ell_{j,t}, h_j \geq 0. \end{gathered} \tag{6}$$

Here, $\ell_{j,t}$ denotes removal from the tracked system. Slow recovery remains stored material. The usable balance is

$$m_{t+1} = d_T(1 - \ell_a) m_t + \Delta t\big(q_{r,t} + q_{b,t} - f_t + e_t\big). \tag{7}$$

Decay and stock losses precede transfers; new inflows arrive at interval ends. The causal guard excludes those returns from an earlier withdrawal:

$$\begin{gathered} \Delta t f_t + m_{res} \leq d_T(1 - \ell_a) m_t, \\ 0 \leq f_t \leq \overline{f}, 0 \leq q_{j,t} \leq \overline{q}_j, m_{res} \leq m_t \leq \overline{m}. \end{gathered} \tag{8}$$

This convention is conservative within an interval. Total stock and its independent balance are

$$M_t = m_t + \sum_j 1^T x_{j,t}, M_t \leq \overline{M}. \tag{9}$$

$$\begin{gathered} M_{t+1} = d_T M_t + \Delta t[(B-1) b_t + e_t - L_t), \\ L_t = \frac{d_T}{\Delta t}\left(\ell_a m_t + \sum_j \ell_{j,t}^T x_{j,t} \right). \end{gathered} \tag{10}$$

Internal transfers cancel. Only breeding, burning, external supply, decay, and declared losses change total mass. Compartment order remains fixed during identification. The transition model describes an unsaturated processing envelope, with return capacities imposed as feasibility constraints. A slowdown reduces the transfer fraction and retains the delayed mass upstream. Its immediate effect is a change in material availability within the conserved total stock.

For constant matrices, the corresponding kernel and response are

$$a_{j,l} = d_T^l c_j^T A_j^{l-1} h_j, l \geq 1. \tag{11}$$

$$q_{j,t} = \frac{d_T^{t+1}}{\Delta t} c_j^T A_j^t x_{j,0} + \sum_{l=1}^{t} a_{j,l}\, v_{j,t-l}. \tag{12}$$

The initial-inventory term remains separate from subsequent inflows. The residual kernel mass contains the unresolved residence tail and the accumulated physical losses. The state recursion retains these contributions explicitly when process conditions change.

3.3 Fusion operation and thermal storage

The operating envelope covers production and standby in a thermally ready plant. Production status, transitions, ramps, and dwell periods satisfy

$$\underline{Q} y_t \leq Q_t \leq \overline{Q} y_t, y_t \in \{0,1\}. \tag{13}$$

$$y_t - y_{t-1} = v_t^{+-v_t^-, v_t^{++v_t^- \leq 1, v_t^+, v_t^- \in \{0,1\}.}} \tag{14}$$

$$-R^{-}\Delta t - \overline{Q}v_t^{-} \le Q_t - Q_{t-1} \le R^{+}\Delta t + \overline{Q}v_t^{+}, \tag{15}$$

$$\sum_{i=t-U+1}^{t} v_i^{+} \le y_t, \quad \sum_{i=t-D+1}^{t} v_i^{-} \le 1 - y_t. \tag{16}$$

Prehorizon operating history completes the dwell sums and fixes the initial admissible transitions. Useful heat is allocated by

$$Q_t^h = \eta_h Q_t, \tag{17}$$

$$Q_t^h + H_t^d = H_t^g + H_t^c + H_t^w, H_t^w \ge 0. \tag{18}$$

Auxiliary electricity is not credited as recovered heat. Thermal storage and turbine output obey

$$E_{t+1}^H = \sigma_H E_t^H + \Delta t(\eta_c^H H_t^c - H_t^d/\eta_d^H). \tag{19}$$

$$\begin{gathered} 0 \le E_t^H \le \overline{E}^H, z_t^H \in \{0,1\}, \\ 0 \le H_t^c \le \overline{H}^c z_t^H, 0 \le H_t^d \le \overline{H}^d (1 - z_t^H). \end{gathered} \tag{20}$$

$$P_t^g = \eta_g H_t^g, 0 \le H_t^g \le \overline{H}^g. \tag{21}$$

Stored heat supports electricity only within discharge and turbine limits. Rejected heat leaves the useful-energy boundary. Constant conversion efficiency is a reduced operating approximation.

3.4 Auxiliary power and electrical storage

Auxiliary demand includes standby services, production, fuel processing, and hot restart energy:

$$\begin{aligned} P_t^a = P_0 + P_y y_t + \chi_Q Q_t + \chi_f f_t \\ + \chi_r(q_{r,t} + q_{b,t}) + E_{st} v_t^{+/\Delta t}. \end{aligned} \tag{22}$$

Flow coefficients have units of MWh/kg. Processing can consume electricity while fusion production is inactive. The battery balance, its limits, and net grid exchange are

$$E_{t+1}^B = \sigma_B E_t^B + \Delta t(\eta_c^B P_t^c - P_t^d/\eta_d^B), \tag{23}$$

$$\begin{gathered} \underline{E}^B \le E_t^B \le \overline{E}^B, z_t^B \in \{0,1\}, \\ 0 \le P_t^c \le \overline{P}^c z_t^B, 0 \le P_t^d \le \overline{P}^d (1 - z_t^B). \end{gathered} \tag{24}$$

$$P_t = P_t^g - P_t^a + P_t^d - P_t^c. \tag{25}$$

Positive exchange denotes export. Delivery deviations remain explicit:

$$P_t + \delta_t^{-} - \delta_t^{+} = D_t, \delta_t^{-}, \delta_t^{+} \ge 0, -\overline{I} \le P_t \le \overline{P}. \tag{26}$$

Imports are prohibited in the principal benchmark. A throughput charge discourages unnecessary cycling:

$$C_t^{deg} = c_B \Delta t(P_t^c + P_t^d). \tag{27}$$

The linear charge assigns an operating cost to each unit of battery throughput. Charge and discharge energy are also retained as physical measures of storage use.

4. Constrained Learning of Delays and Hidden Inventories

4.1 State representation and measurements

The physical state X_t contains usable fuel, route stocks, and stored energy. Augmented state z_t adds sensor biases and delayed-measurement history. Parameters θ specify transfer fractions within a fixed graph:

$$z_{t+1} = F_\theta(z_t, u_t, w_t). \tag{28}$$

Process uncertainty changes admissible transfers or declared boundary flows, preserving mass in every realization. Observations satisfy

$$o_t = h_\theta\left(z_{t-\delta_o}, u_{t-\delta_o}\right) + d_t + \epsilon_t. \tag{29}$$

Channel-specific delays are represented by the alignment map δ_o. Bias has a bounded, slowly varying prior; random noise has covariance R_o. A return-flow reading does not identify the remaining upstream distribution.

4.2 Constrained identification and local sensitivity

Offline fitting uses complete training sequences, constrained by physical transitions, nonnegativity, parameter bounds, and measurement timing:

$$\begin{aligned} \min_{\theta,\{z\}} \sum_{k\in T_{tr}} \|o_k - \hat{o}_k)^2_{R_o^{-1}} + \lambda_\theta \|\theta - \theta_0)^2 \\ +\lambda_m \sum_{(k,h)\in V_{tr}} \frac{\left(m^{obs}_{k+h} - \hat{m}_{k+h\vee k}\right)^2}{\sigma_m^2}. \end{aligned} \tag{30}$$

The multistep inventory term regularizes accumulated flow error alongside the measurement misfit. Prediction pairs in V_{tr} belong to the training histories. Similar admissible minima retain alternative state–parameter combinations consistent with the observations.

With free parameters, initial hidden stocks, and biases collected in ξ, local sensitivity is

$$G = \sum_{k\in T_{tr}} J_k^T R_o^{-1} J_k, J_k = \frac{\partial \hat{o}_k}{\partial \xi}. \tag{31}$$

Small singular values identify combinations of parameters, hidden stocks, and biases with similar local observation responses. Constant feed reduces information about residence dynamics because transient responses carry the timing signal. The fixed compartment graph retains uncertainty along weakly observed directions. Admissible operating changes excite these dynamics, while separate return channels distinguish routes whose inflows remain proportional at fixed burn fraction. Multistep inventory prediction measures the accumulated consequence of those directions.

4.3 Joint Bayesian state estimation

For arrived information D_t, the joint posterior follows

$$\begin{aligned} \pi_t(z,\theta) \propto p(o_t|z,\theta) \\ \times \int p(z|z', u_{t-1}, \theta)\pi_{t-1}(z',\theta)dz'. \end{aligned} \tag{32}$$

Stored history supplies the likelihood for delayed channels. A bootstrap particle approximation propagates physically admissible states and updates weights:

$$\omega_t^{(s)} = \frac{\omega_{t-1}^{(s)} p\left(o_t|z_t^{(s)}, \theta^{(s)}\right)}{\sum_i \omega_{t-1}^{(i)} p\left(o_t|z_t^{(i)}, \theta^{(i)}\right)}. \tag{33}$$

Resampling controls weight concentration. Parameter moves preserve the transfer structure and use posterior acceptance probabilities. Constrained moving horizon estimates provide admissible initial states [23]. Each likelihood update includes the channels available at that time, with source timestamps retained for delayed readings.

Sensor residuals provide a further check on model interpretation. A persistent stock offset with accurate return measurements differs from a simultaneous decline in measured flow and usable inventory. The bias prior attributes persistent measurement offsets to the observation model, while the process state carries material retention. During a channel outage, the transition equations propagate the hidden stocks and their uncertainty. A smooth conditional mean can therefore coexist with a widening range of admissible fuel distributions.

For a fixed control sequence, predictive lower bounds and risk allocation satisfy

$$\underline{m}_{k\vee t} = F^{-1}_{m_{t+k}|D_t,u}(\alpha_k). \tag{34}$$

$$P\left(\bigcup_{k=1}^{H}\{m_{t+k} < \underline{m}_{k\vee t}\}|D_t, u\right) \le \sum_{k=1}^{H} \alpha_k \le \varepsilon. \tag{35}$$

The union bound applies to valid conditional marginal bounds for the selected control sequence and allows temporal dependence. Its total risk allocation covers the entire path. Marginal coverage measures individual forecast points, while complete-path coverage measures whether every point in a forecast window satisfies its interval.

4.4 Decision-dependent trajectory generation

Each scenario retains dependence among current stocks, parameters, biases, and future process conditions:

$$\left(z_t^{(s)}, \theta^{(s)}, w_{t:t+N-1}^{(s)}\right) \sim p(z_t, \theta, w_{t:t+N-1} | D_t). \tag{36}$$

Propagation inside the dispatch constraints makes future fuel returns depend on the common throughput sequence. The current information set contains only measurements that have already arrived. After applying the first action, new observations update the estimator. Calibration separately scores steady operation, inventory depletion, and recovery because average coverage can conceal poor protection near the withdrawal boundary.

5. Coordinated Dispatch and Deliverability Analysis

5.1 Cost, risk, and causal decisions

Scenario cost includes heat production, starts, battery throughput, and delivery deviations:

$$C_s = \sum_{k=0}^{N-1} \tag{37}$$

Heat cost uses thermal MWh; deviation prices use electrical MWh. Common delivery requirements prevent reduced service from appearing as successful coordination. Expected cost and shortage risk are combined as

$$min \sum_s w_s \, C_s + \rho \left(\zeta + \frac{1}{1-\alpha} \sum_s w_s \, \xi_s \right), \sum_s w_s = 1. \tag{38}$$

The auxiliary variables represent conditional value at risk [36]:

$$L_s = \Delta t \sum_{k=0}^{H-1} \delta_k^{-,(s)}, \xi_s \geq L_s - \zeta, \xi_s \geq 0. \tag{39}$$

The weight ρ monetizes shortage energy. Fuel protection imposes a separate joint requirement:

$$\begin{gathered} g_k = max\{m_{res} - m_k, \\ \Delta t f_k + m_{res} - d_T(1 - \ell_a) m_k\}, \\ P\{g_k \leq 0, k = 0, \dots, N-1 | D_t\} \geq 1 - \varepsilon. \end{gathered} \tag{40}$$

Physical bounds on the retained scenarios form a finite-sample approximation to this joint requirement. The base formulation uses common controls:

$$u_k^{(s)} = u_k \text{for all} s, k = 0, \dots, N-1. \tag{41}$$

Reactor and storage commands cannot use future scenario identities. Returns, auxiliary demand, and delivery deviations remain scenario outcomes. Reoptimization supplies feedback.

5.2 Horizon extension and solution

The delivery horizon H is followed by an extension L, giving $N = H + L$ intervals for continued obligations and inventory recovery. Every scenario satisfies

$$X_N^{(s)} \geq X^{ref}, y_{N-1}^{(s)} = y^{ref}, s \in S. \tag{42}$$

The reference includes each fuel compartment, both stores, and terminal operating history. It prevents late fuel from replacing material expected earlier and limits apparent savings from endpoint depletion. The extension imposes a finite endpoint constraint [33]. Reference conditions remain identical across scheduling cases.

Fixed scenario parameters give linear physical constraints, while equipment modes yield a mixed integer program. The accepted solution is a feasible incumbent together with its objective bound and optimality gap. The controller applies the first common action and updates the horizon after the next observation. A separate physical guard limits withdrawal to the available stock. A rejection records a requested action beyond that limit; a realized violation

records an executed transition below the reserve. These indicators separate command generation from the effect of protection.

5.3 Deliverability bounds and inventory timing

Let W denote the delivery window and Ξ the declared finite scenario set. Constant delivery capacity is

$$\begin{gathered} C_W(X_0,\Xi) = \max_{d,u} d, \\ \text{subject to} D_k = d, \delta_k^- = 0, k < W, \\ (X,u) \in F(\Xi). \end{gathered} \tag{43}$$

The feasible set $F(\Xi)$ retains all physical, common-control, and terminal constraints. Surplus export is allowed; shortage during the delivery window is not. The capacity is conditional on the declared scenario set, delivery window, and terminal reference.

For lossless fuel circulation without external supply, summing usable balances gives the necessary prefix condition

$$\frac{\Delta t}{\beta}\sum_{k=0}^{n-1} b_k \le m_0 - m_{res} + \Delta t \sum_{k=0}^{n-2}\left(q_{r,k} + q_{b,k}\right), n \le W. \tag{44}$$

The last return arrives after the last withdrawal and is excluded. The guard applies to every prefix. With decay and losses, the exact recursion is more restrictive. When imports and delivery shortfall are absent, an optimistic energy bound is

$$\begin{aligned} \Delta t \sum_{k=0}^{W-1} D_k \le \eta_g \eta_h \kappa \Delta t \sum_{k=0}^{W-1} b_k + \eta_g \eta_d^H E_0^H \\ + \eta_d^B E_0^B - \Delta t \sum_{k=0}^{W-1} P_k^a . \end{aligned} \tag{45}$$

This bound assumes nonnegative terminal energy and efficiencies and retention factors no greater than unity. Discarding charging losses and unused energy makes it optimistic; discharge and turbine limits can still prevent delivery.

The analytical example uses a lossless hourly chain that returns its first compartment at each interval end. Usable stock is 0.20 kg, the reserve is 0.05 kg, and each requested withdrawal is 0.15 kg. New recycling and breeding inflows cannot return during the first two intervals. The initial states satisfy

$$\begin{gathered} x_{r,0}^A = (0.15, 0.15, 0)^T, x_{r,0}^B = (0,0,0.30)^T, \\ M_0^A = M_0^B = 0.50, m_1^A = 0.20, m_1^B = 0.05. \end{gathered} \tag{46}$$

For cumulative returns $R_0^A(n)$ and $R_0^B(n)$ from initial stocks, the lossless subsystem gives

$$R_0^A(n) \ge R_0^B(n) \forall n \Rightarrow F_B \subseteq F_A. \tag{47}$$

Equal usable stock and identical kernels make induced returns identical for a common withdrawal sequence. Earlier initial returns preserve every withdrawal sequence feasible under later returns, provided upper stock and return-flow limits remain inactive. The inclusion concerns fuel feasibility. In the electrical balance, differing returns also change processing auxiliaries through (22), so the coupled delivery calculation retains that additional load.

Bounded long-run operation requires

$$(B-1)\overline{b} + \overline{e} \ge \frac{1 - d_T}{\Delta t}\overline{M} + \overline{L}. \tag{48}$$

Bars denote time averages. Storage shifts energy delivery but cannot supply tritium missing from a sustained fuel deficit.

5.4 Conservation and reliability verification

Independent accounting checks use

$$r_t^M = M_{t+1} - d_T M_t - \Delta t[(B-1)b_t + e_t - L_t). \tag{49}$$

$$r_t^E = \begin{bmatrix} Q_t^h + H_t^d - H_t^g - H_t^c - H_t^w \\ P_t^g - P_t^a + P_t^d - P_t^c - P_t \\ (E_{t+1}^H - \sigma_H E_t^H)/\Delta\, t - \eta_c^H H_t^c + H_t^d/\eta_d^H \\ (E_{t+1}^B - \sigma_B E_t^B)/\Delta\, t - \eta_c^B P_t^c + P_t^d/\eta_d^B \end{bmatrix}. \tag{50}$$

Thermal and electrical residuals use their respective rated-power scales. A transition passes the accounting check when each residual lies within its tolerance. Reliability treats each independent episode as one trial. For k_v events in n_v independent trials under fixed settings, the exact one-sided upper limit is [37]

$$p_U = \begin{cases} F^{-1}_{Beta(k_v+1, n_v-k_v)}(1-\gamma), & k_v < n_v, \\ 1, & k_v = n_v. \end{cases} \tag{51}$$

Its confidence level is $1-\gamma$ for the episode-generating distribution. Separate indicators count rejected requests and realized reserve violations. A solver bound measures the remaining optimization gap, an episode confidence limit measures event-frequency uncertainty, and a balance residual measures accounting accuracy. Each quantity therefore has a distinct interpretation in the coupled material and energy calculation.

6. Data and Parameters

6.1 Benchmark construction and operating inputs

The study uses a numerical design benchmark. Table 3 identifies the structural sources and the operating assumptions. TMAP8 supplies the compartment reference [13], while Power Balance Models define the separation of generation and auxiliary demand [15].

Table 3 Provenance and use of benchmark information

Source	**Information used**	**Role**
Fuel cycle literature [5], [6], [11]	Separate fuel sources, residence, and retained inventories	Fuel transport structure
TMAP8 example [13]	Published compartment benchmark and selected fuel ratios	Compartment formulation
UKAEA PBM [16]	Gross generation and auxiliary load separation	Power accounting boundary
RTS-GMLC [39], [40]	Chronological demand and renewable profiles	Chronological benchmark context
Present benchmark	Delivery schedule, noise, process changes, storage and cost settings	Numerical case definition

Episodes last 72 h, with a repeated delivery schedule and an imposed recycling slowdown. These signals are defined independently of the compared command profiles.

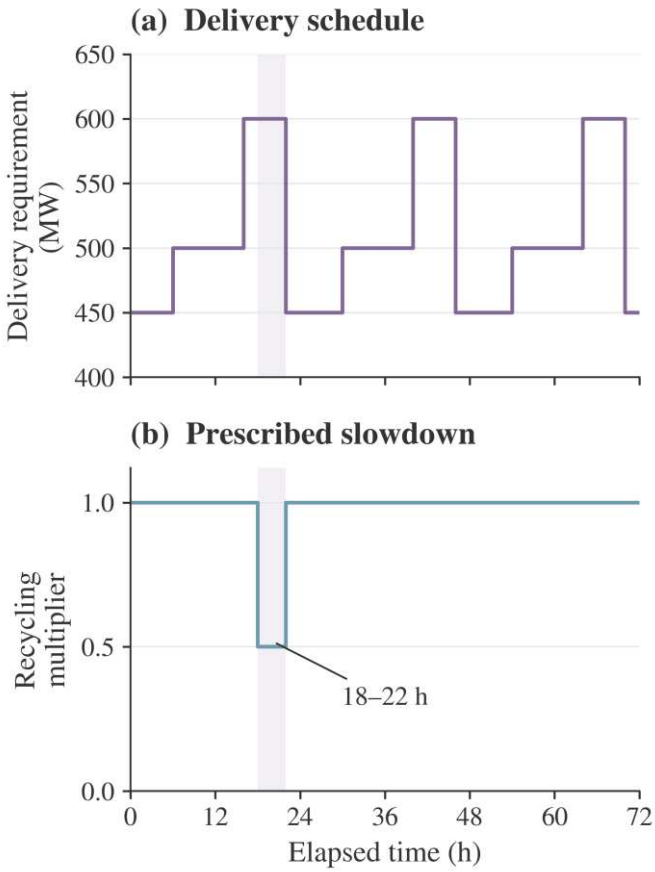

Fig. 2 Declared delivery schedule and imposed recycling slowdown. The daily requirement is 12,200 MWh; the process multiplier is an input assumption

Fig. 2 places the fuel-processing event within the daily electricity requirement. The target increases from 450 MW to 600 MW before returning to its overnight level. Each day requires 12,200 MWh, giving every command profile the same cumulative obligation. The recycling multiplier falls to one half between hours 18 and 22, overlapping the evening plateau. This overlap concentrates the demand for stored energy within a period of reduced fuel recovery. The breeding route retains its nominal transfer setting, so the disturbance has a defined material origin. Slower transfer holds tritium in the recycling compartments and reduces the portion reaching usable storage. The repeated demand pattern also separates the event from ordinary daily variation. Subsequent recovery occurs under the same delivery schedule, exposing the competition between replenishing inventory and supporting the next high-demand period.

Chronological test systems such as RTS-GMLC preserve the ordering of demand and renewable generation [38], [39]. The controlled schedule used here retains an explicit daily sequence with fixed plateau levels. Its construction isolates the overlap between peak delivery and interrupted fuel recovery, independently of changes in grid composition. All plotted delivery values follow this specified schedule.

6.2 Fuel parameters and initial conditions

Table 4 gives the temporal and fuel settings. Effective burn fraction and breeding ratio match the documented TMAP8 example. The energy constant follows the reaction energy per tritium nucleus. Tritium decay uses the evaluated half-life [40]; the other values are benchmark assumptions.

Table 4 Fuel cycle and temporal parameters

Parameter	Value	Basis
Interval Δt	0.25 h	Assumed
Delivery horizon H	96 intervals	Assumed

Parameter	Value	Basis
Extension L	96 intervals	Assumed
Effective burn fraction β	0.025	[13]
Breeding ratio B	1.067	[13]
Energy constant κ	$1.56 \times 10^5\ MWh_{th}$/kg	Derived
Tritium half life	12.32 years	[41]
Recycling stages; p_r	3; 0.50	Assumed
Breeding stages; p_b	4; $1/6$	Assumed
Nominal mean residence	1.5 h; 6 h	Derived
Stage loss fraction ℓ_j	10^{-5}/interval	Assumed
Usable loss fraction ℓ_a	10^{-6}/interval	Assumed
Initial usable stock m_0	0.60 kg	Assumed
Usable reserve m_{res}	0.05 kg	Assumed
Usable capacity $\overline{m}$	3.0 kg	Assumed
Total stock capacity $\overline{M}$	10.0 kg	Assumed
Feed capacity $\overline{f}$	0.70 kg/h	Assumed
Return capacities $\overline{q}_r, \overline{q}_b$	0.80; 0.05 kg/h	Assumed
External supply e_t	0 kg/h	Fixed boundary
Terminal usable reference	0.30 kg	Assumed

New route inflow enters the last compartment. The diagonal of A_j is $1 - p_j - \ell_j$, its superdiagonal is p_j, and only the first entry of c_j equals p_j. The lossless mean residence is the stage count multiplied by $\Delta t/p_j$.

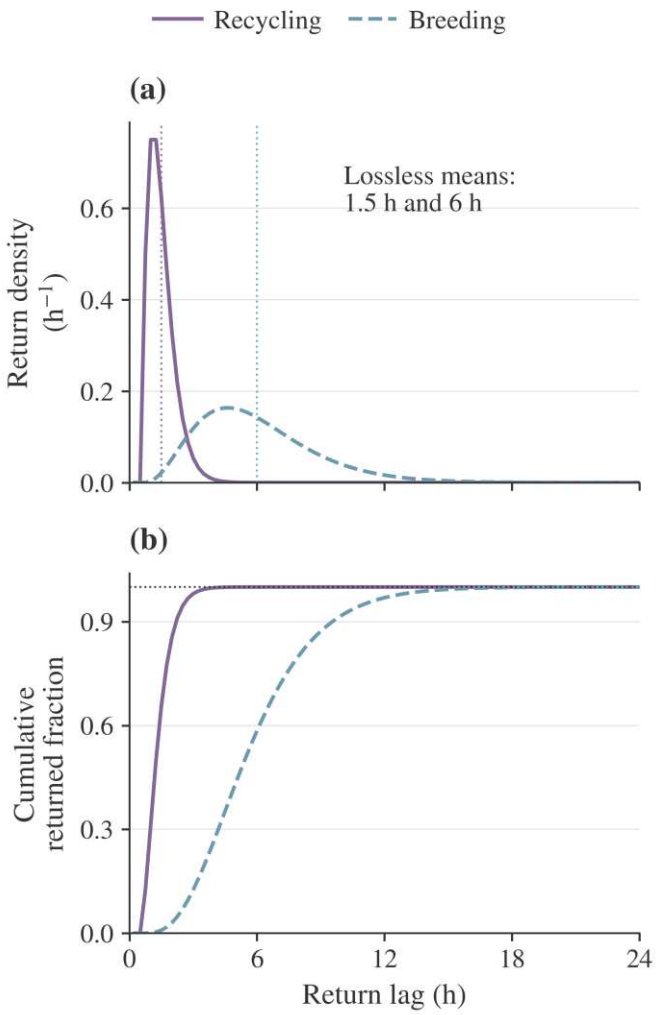

Fig. 3 Nominal recycling and breeding return kernels calculated from the compartment matrices. Losses are retained; marked means refer to lossless chains

Fig. 3 resolves the delay between route entry and fuel recovery. The recycling kernel concentrates its return earlier, while the longer breeding chain spreads recovery across a wider interval. The marked means of 1.5 h and 6 h characterize lossless residence times. Their locations differ from the density peaks because the return distribution is asymmetric. Material entering the last compartment passes through each preceding stage before reaching the outlet, producing a finite earliest return. The cumulative curves therefore contain information that a mean delay alone omits. Their early slopes determine the fuel recovered before a near-term withdrawal; their tails determine the inventory still in transit during later commitments. Decay and processing losses remain in the calculation, so cumulative recovery stays below the injected mass.

Initial route stocks solve the nominal steady balance at 1500 MW_{th}. Terminal route references equal those vectors; usable stock starts at 0.60 kg and has a 0.30 kg terminal reference. Both stores start at 60% capacity. The optimization formulation sets that fraction as their terminal lower bound. Initial operation meets its dwell time requirement, and the final production status is one.

6.3 Energy resources and observation protocol

Table 5 specifies conversion, storage, auxiliaries, and costs. Start energy describes a hot transition. Imports and external tritium supply remain zero. Duration scans vary energy capacity at fixed power; ablations remove both ratings and initial energy of an absent store.

Table 5 Plant conversion, storage, and cost parameters

Parameter	Assumed value
Fusion heat range $\underline{Q}, \overline{Q}$	700–2000 MW_{th}
Heat ramps $R^{+,R^{-}}$	1000 MW_{th}/h
Minimum production; standby	2 h; 1 h
Heat recovery η_h; turbine η_g	0.92; 0.42
Turbine heat capacity $\overline{H}^{g}$	2200 MW_{th}
Thermal capacity $\overline{E}^{H}$	3000 MWh_{th}
Thermal charge and discharge limits	1000 MW_{th} each
Thermal efficiencies η_c^H, η_d^H	0.98; 0.98
Thermal retention σ_H	$exp(-0.001\Delta t)$
Battery capacity $\overline{E}^{B}$	800 MWh
Battery minimum $\underline{E}^{B}$	80 MWh
Battery charge and discharge limits	200 MW each
Battery efficiencies η_c^B, η_d^B	0.95; 0.95
Battery retention σ_B	$exp(-0.0001\Delta t)$
Auxiliary loads P_0, P_y	20 MW each
Heat dependent auxiliary χ_Q	0.05 MW/MW_{th}
Flow auxiliaries χ_f, χ_r	5; 2 MWh/kg
Start energy E_{st}	5 MWh
Export limit $\overline{P}$; imports $\overline{I}$	900 MW; 0 MW
Heat operation cost c_Q	2 \$/MWh_{th}
Start cost c_{st}	5000 \$/start
Battery throughput cost c_B	6 \$/MWh
Shortfall; excess prices c_-, c_+	1000; 20 \$/MWh
CVaR level α; weight ρ	0.95; 200 \$/MWh
Fuel risk target ε	0.01 per horizon

The master seed is 20260909. Episode transfer fractions vary uniformly within twenty percent of nominal values. The observation protocol assigns separate histories to training, calibration, and validation. Sensor errors combine independent Gaussian noise with persistent bias drawn uniformly within two channel standard deviations. Inventory noise has a standard deviation of 0.005 kg and a fifteen-minute observation delay. Feed, recycling-return, and breeding-return noise standard deviations are 0.007, 0.008, and 0.0005 kg/h, respectively. Hidden route stocks are withheld from the estimator. The algorithm specification uses 512 particles, 64 joint scenarios, and resampling below half the population. The fitting objective scales parameters by their prior widths and uses separate inventory and parameter regularization. The reference observation protocol assigns 120 training, 40 calibration, and 300 validation histories. Generated cohorts contain 60 or 24 episodes, as specified in Table 7. Forecast windows span 1, 4, and 12 h. The scenario process assigns a slowdown-entry probability of 0.01 per interval and a recovery probability of $1/16$. The imposed-event simulations fix the slowdown interval. The scheduling specification uses a relative gap of 10^{-3} and a 60 s update limit.

6.4 Command profiles and numerical datasets

The dispatch simulations apply prescribed thermal commands to the fuel and storage balances. Profiles A–D share a demand-following component and a daily sinusoid. Before ramp and output limits, the command is $(D_t + 43)/0.3364 + 135sin[2\pi\,(t + \phi)/24) + a_i - b_i I_t$ in MW_{th}, where t is measured in hours, ϕ is uniform on $[-0.5, 0.5)$ h, and I_t marks hours 18.5–23. Table 6 specifies the profile coefficients. Paired episodes share transfer

fractions and phase. The causal guard limits executed feed to stock above the reserve. During a heat deficit, thermal storage supplies 72% of the requested heat support when both stores are present; the battery supplies the remaining electrical deficit within its limits. Thermal storage supplies the full requested heat support when used alone. These finite-episode trajectories end at their evolved inventories, without the terminal reset used in the optimization formulation.

Table 6 Prescribed command profiles used in the dispatch simulations

Profile	a_i (MW_{th})	b_i (MW_{th})
A	0	150
B	-75	250
C	40	0
D	100	-70

Table 7 defines the construction of each numerical dataset. The command-driven trajectories follow the physical recursion. The uncertainty bands and parametric response grids are synthetic calculations with explicit generation rules. Mass checks use a tolerance of 10^{-8} kg; scaled heat and electricity checks use 10^{-6}. Storage-energy residuals are divided by the interval length before power scaling.

Table 7 Numerical datasets and their construction

Dataset	**Construction**	**Calculated quantity**
Operating inputs	Defined schedule, compartment matrices, sensor specification	Demand, return kernels, initial stocks
Analytical example	Lossless hourly chain	Causal withdrawals
Dispatch trajectories	Prescribed commands; 60 paired episodes, 24 for storage ablation	Delivery, inventories, cost, rejected requests
Uncertainty experiments	Synthetic bands and correlated errors; 60 forecast paths	Interval width and coverage
Sensitivity responses	Specified response laws; 24 realizations	Duration, noise, and slowdown effects

7. Numerical Results and Discussion

7.1 Paired comparisons and uncertainty summaries

All comparisons retain episode identities. Mean-outcome intervals use 2000 percentile bootstrap resamples of whole episodes, with seed 20260910, following Efron [41]. Paired comparisons reuse the same resampled identities across cases, preserving dependence within each history. Event limits use (51). Missing outcomes remain unscored. Dispatch profiles A–D refer to Table 6; synthetic experiments follow the constructions in Table 7. The resulting intervals quantify variation under each specified data-generating process.

7.2 Dispatch trajectory and withdrawal protection

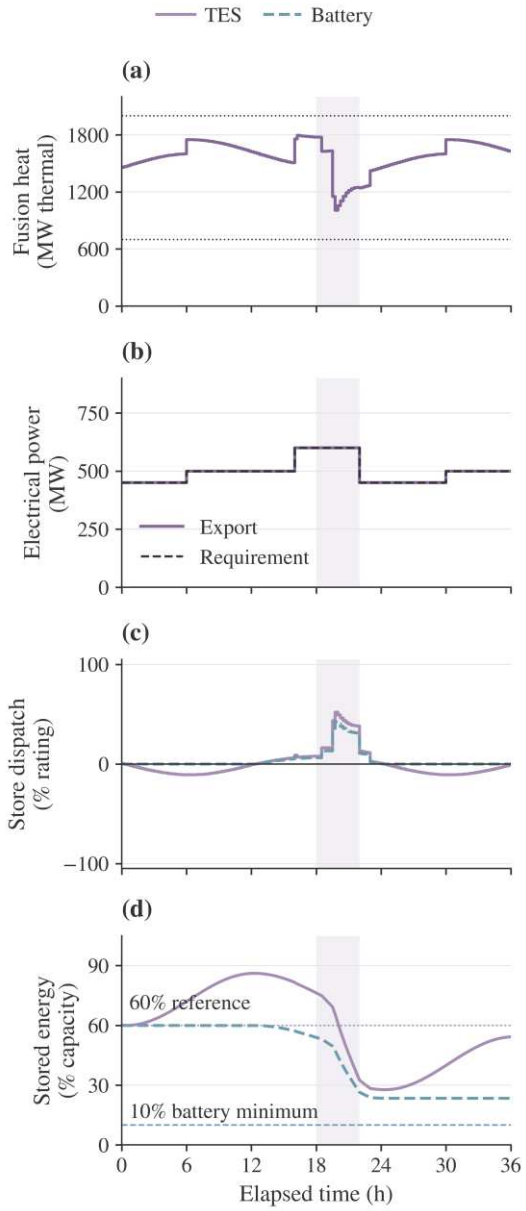

Fig. 4 Protected command-driven trajectory for profile A, episode 001. Positive normalized storage power denotes discharge

Fig. 4 follows profile A through the first 36 h of the prescribed-command simulation. Fusion heat varies between approximately 1008 and 1794 MW_{th}, while net delivery follows the 450–600 MW requirement throughout this excerpt. The difference between heat production and delivered electricity is resolved by conversion, auxiliary demand, and storage exchange. During a deficit, thermal discharge supports turbine input and the battery supplies the remaining electrical requirement. Each normalized storage trace uses its own device rating, preserving the distinction between thermal and electrical power. Battery energy decreases from 480 MWh to approximately 187 MWh before rising again within the plotted history. Usable fuel simultaneously reaches a minimum of about 0.115 kg. Exact delivery tracking thus coexists with substantial movement of the fuel and storage inventories.

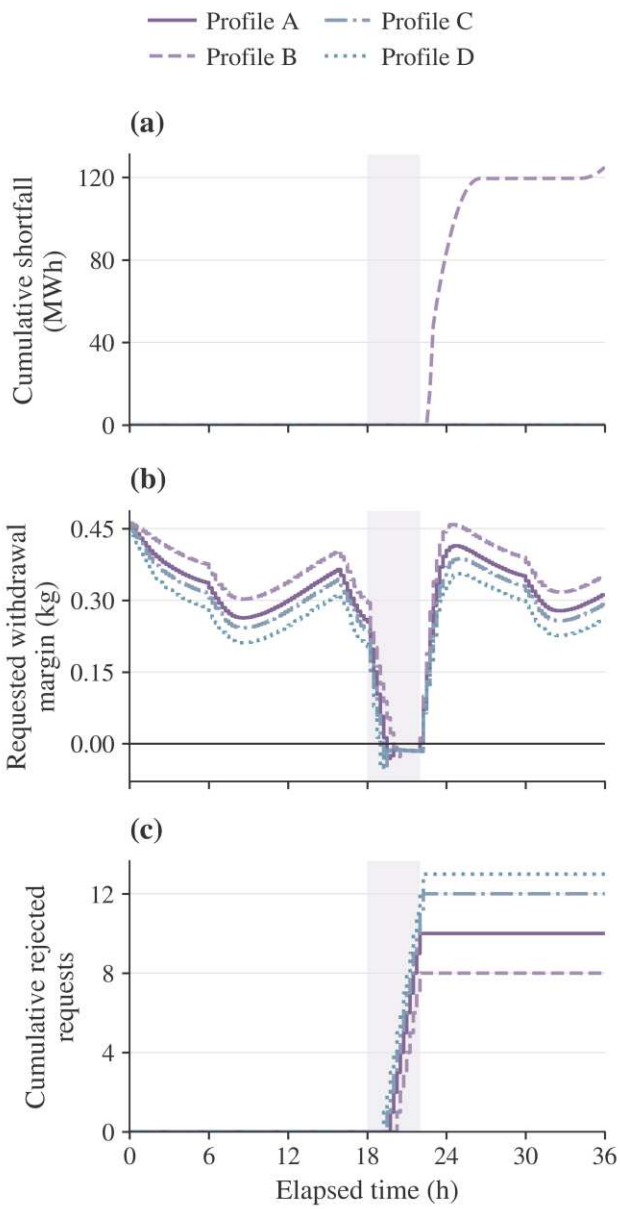

Fig. 5 Requested fuel margins, delivery loss, and rejected withdrawals under paired command profiles

Fig. 5 links requested fuel margins to protected operation and delivery loss. A negative margin identifies a command that reaches beyond usable stock after reserving the minimum inventory. The causal guard reduces executed withdrawal at those points, so the displayed traces contain no realized reserve violation. Profiles A–D record 10, 8, 12, and 13 rejected requests, respectively. Profile B accumulates approximately 124.9 MWh of shortfall during the excerpt, while the other profiles maintain the delivery requirement. Its smaller rejection count accompanies a larger loss of service because lower requested production also limits the energy available to the turbine and stores. Rejection frequency and delivery loss thus describe different aspects of operation. The cumulative curves preserve when each consequence occurs, linking the imposed recycling slowdown to subsequent recovery. Protection enforces the fuel boundary; available storage determines how much of the resulting production reduction reaches the grid.

7.3 State uncertainty and forecast coverage

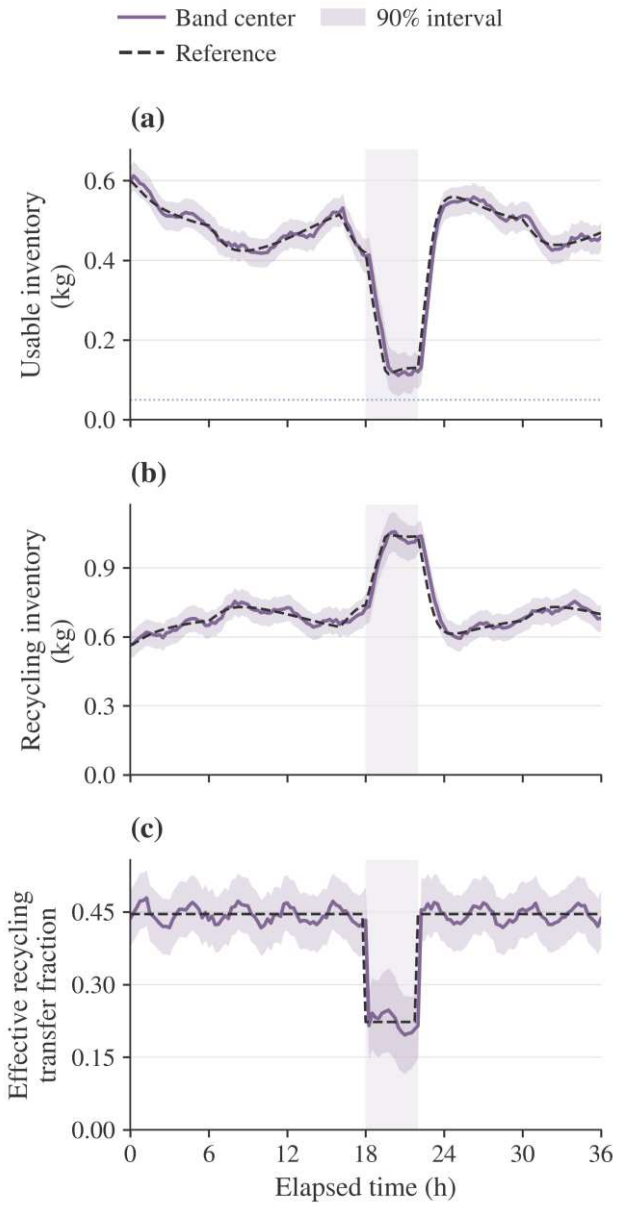

Fig. 6 Synthetic state and transfer-fraction bands about the selected trajectory. Ribbons denote central marginal intervals

Fig. 6 examines a synthetic uncertainty construction around the selected physical trajectory. Its central curves combine a one-interval lag with oscillatory and random errors. The usable-stock, aggregate recycling, and effective-transfer panels therefore expose different consequences of delayed information. Usable inventory governs the immediate withdrawal margin, whereas recycling inventory records material awaiting release. During the imposed slowdown, the effective transfer fraction drops even as retained route material accumulates. The widening bands around that transition express the specified increase in uncertainty during a process change. After recovery, the route stock and usable stock adjust on different time scales because transfer moves material between them. The recycling panel summarizes the total route inventory rather than the individual compartments. This distinction links an observable aggregate to the unresolved maturity distribution that controls later returns.

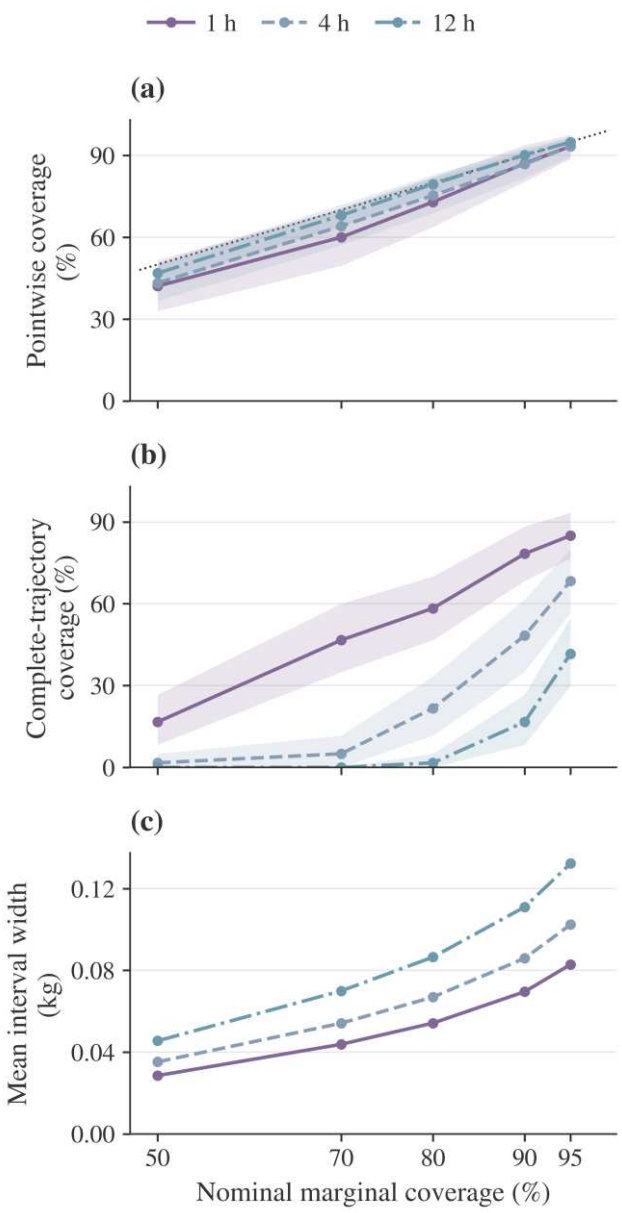

Fig. 7 Marginal and complete-path coverage under correlated synthetic forecast errors. Shading denotes whole-episode bootstrap intervals

Fig. 7 quantifies coverage under temporally correlated synthetic forecast errors. At nominal 90% coverage, the pointwise scores are approximately 87.1%, 86.8%, and 90.2% for the 1, 4, and 12 h windows. Complete-path coverage decreases from 78.3% to 48.3% and then 16.7%. A longer path contains more opportunities to cross an interval boundary, even when individual points retain similar coverage. Mean interval widths increase from approximately 0.070 kg to 0.111 kg across those windows, so widening marginal bands does not eliminate the path-level effect. Whole-episode resampling retains the serial dependence of each error sequence. The comparison gives a direct interpretation of the risk allocation in (35): the relevant event for fuel availability concerns the whole withdrawal sequence. An average pointwise score describes a different event and therefore carries different information for an uninterrupted delivery commitment.

7.4 Storage allocation and ablation

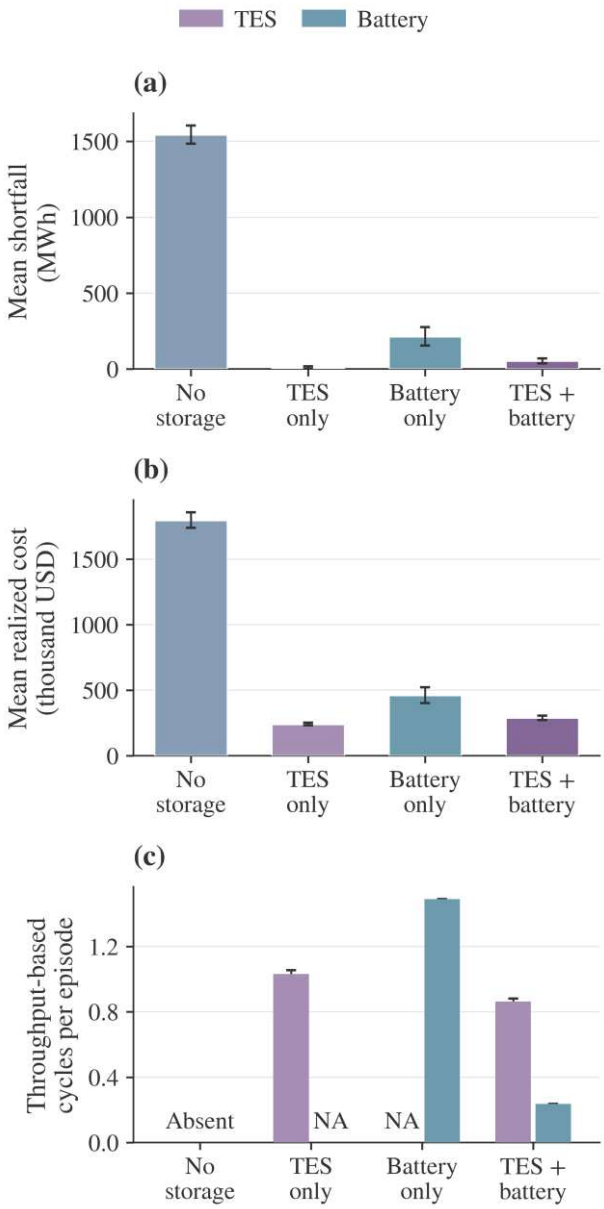

Fig. 8 Storage ablation under prescribed allocation. Device removal also removes its initial energy; NA identifies an absent store

Fig. 8 resolves the effect of storage configuration under the prescribed allocation rule. Mean shortage is approximately 1542.4 MWh without storage, 7.1 MWh with thermal storage, 213.3 MWh with the battery, and 53.6 MWh with both. Thermal storage alone gives the lowest shortage in this comparison. The combined rule assigns part of the deficit to the battery, so its outcome depends on the timing of battery depletion as well as the available thermal energy. Adding a device therefore changes the executed allocation, not only the installed capacity. Device removal also removes its initial charge, making the comparison sensitive to both flexibility and the starting energy endowment. The cycle panel expresses throughput relative to each installed store's capacity. Undefined entries identify absent devices. Final inventories carry the energy consequences of earlier delivery support.

7.5 Storage-duration response

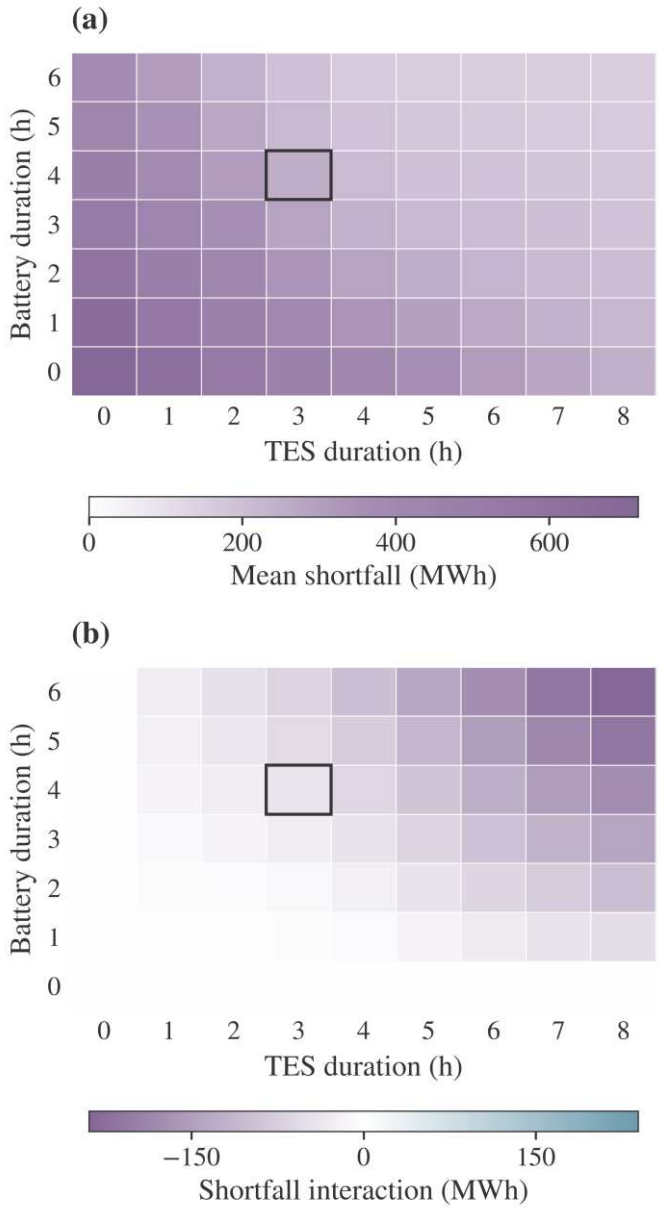

Fig. 9 Synthetic storage-duration response and paired interaction. The outlined cell marks the base configuration

Fig. 9 evaluates the specified synthetic shortage response across thermal and battery durations at fixed power ratings. Mean shortage decreases from approximately 716.0 MWh at zero duration to 249.6 MWh at the base combination of 3 h thermal and 4 h battery duration. The separate base-duration cases yield approximately 459.3 and 466.6 MWh. Their reductions overlap: the joint reduction is smaller than the sum of the individual reductions. The interaction measure, defined as the joint reduction minus the separate reductions, is approximately −39.7 MWh at the base cell. Zero-duration edges have zero interaction because only one resource contributes there. The smooth response follows the stipulated duration law and its shared episode multiplier. Holding the initial charge fraction constant also increases starting energy with duration. Decreasing shortage and additional joint benefit are separate response properties.

7.6 Measurement and disturbance sensitivity

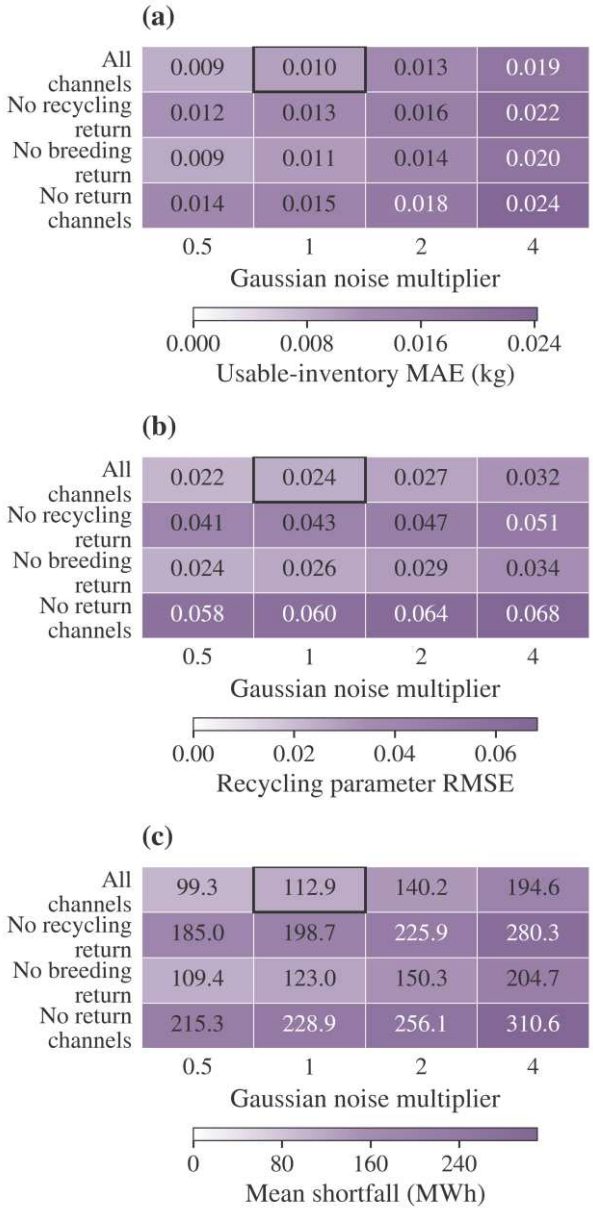

Fig. 10 Synthetic sensor-channel and noise sensitivity with inventory and feed measurements retained in each case

Fig. 10 compares the specified synthetic error responses to return-channel availability and Gaussian noise. Inventory and feed measurements remain in every configuration, and the persistent-bias scale stays fixed. At the base noise level, the all-channel usable-stock error is approximately 0.0101 kg and the recycling-parameter error is approximately 0.0241. Removing the recycling return channel raises the latter to approximately 0.0432, while removing the breeding return channel gives approximately 0.0261. The construction assigns the strongest recycling-parameter penalty to losing its direct return observation. Increasing the noise multiplier raises all error measures, with a different response law for parameter error than for inventory error. The shortfall panel uses the same episode multiplier but a separate channel penalty. This separation makes the assumed relationship between information quality and delivery loss explicit.

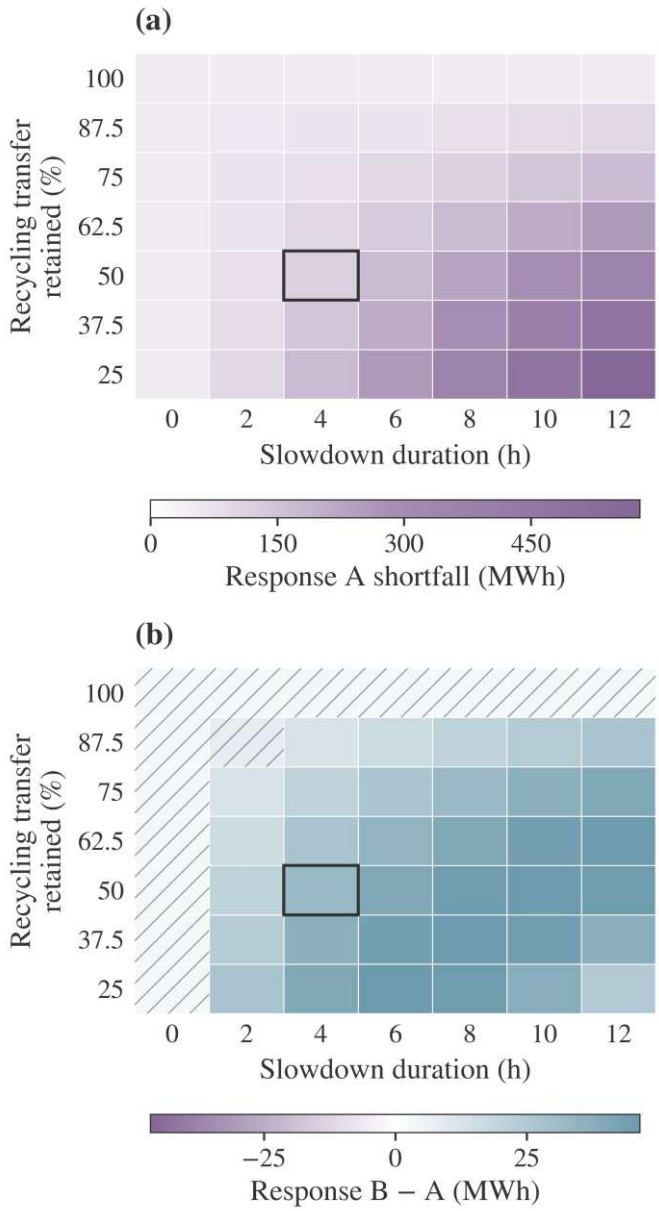

Fig. 11 Synthetic slowdown responses and paired differences. Hatching identifies intervals containing zero

Fig. 11 evaluates synthetic slowdown responses using severity equal to event duration multiplied by the lost transfer fraction. A longer interruption and a smaller retained fraction both increase severity. Response A assigns a superlinear shortage increase to this quantity, producing the strongest losses toward the prolonged, deep-slowdown corner. Response B adds a severity-dependent difference and a paired episode perturbation. The difference panel consequently changes according to the specified response laws, while matched sampling removes unrelated variation between the compared records. The zero-duration and unchanged-transfer edges share the no-event severity value. Hatched cells identify paired intervals containing zero, distinguishing the estimated direction of the difference from its sampling uncertainty. The outlined base event lies within the scan, connecting the imposed disturbance in Fig. 2 to the wider severity range.

The present estimator uses fuel inventory and flow measurements. An extension using optical event streams would require a link between a camera signal and a measurable fuel-cycle quantity, such as return flow. PRE-Mamba illustrates how rain-induced noise can be filtered from event-camera data [42], and EventPrune uses event-derived motion cues to select visual

inputs for video reasoning [43]. Whether either preprocessing method would preserve the signal needed to estimate fuel flow remains to be tested.

8. Conclusion

Fuel maturity determines how much of a fusion plant's inventory supports an immediate delivery commitment. The compartment formulation preserves this timing information and connects it to state estimation, thermal storage, battery operation, and net electricity. The causal withdrawal condition separates available fuel from material returning later. In the analytical example, both initial states contain 0.50 kg, but only the earlier-return state supplies consecutive 0.15 kg requests while preserving the reserve. The complementary energy bound accounts for fuel conversion, auxiliary demand, and precharged storage within the same delivery window.

The 72 h benchmark resolves the operational consequences of this timing constraint. Protected command simulations distinguish rejected requests from realized fuel violations and connect the resulting production changes to electricity shortfall. Storage allocation changes both discharge timing and the resources remaining at the episode endpoint. The synthetic forecast calculation further shows that similar marginal coverage can accompany sharply different complete-path coverage. These findings place material timing, energy transfer, and temporal uncertainty within a common dispatch formulation. Dependable delivery requires their simultaneous satisfaction: sufficient total fuel or aggregate stored energy alone does not establish availability at each scheduled withdrawal.

References

[1] J. A. Schwartz, W. Ricks, E. Kolemen, and J. D. Jenkins, The value of fusion energy to a decarbonized United States electric grid, Joule 7(4), 675–699 (2023). https://doi.org/10.1016/j.joule.2023.02.006

[2] L. Breuning, A. Kerekeš, A. von Müller et al., Operational planning of magnetic confinement fusion power plants using a MIP unit-commitment model, Fusion Eng. Des. 222, 115316 (2026). https://doi.org/10.1016/j.fusengdes.2025.115316

[3] R. J. Pearson, A. B. Antoniazzi, and W. J. Nuttall, Tritium supply and use: a key issue for the development of nuclear fusion energy, Fusion Eng. Des. 136, 1140–1148 (2018). https://doi.org/10.1016/j.fusengdes.2018.04.090

[4] M. Kovari, M. Coleman, I. Cristescu, and R. Smith, Tritium resources available for fusion reactors, Nucl. Fusion 58(2), 026010 (2018). https://doi.org/10.1088/1741-4326/aa9d25

[5] M. Abdou, M. Riva, A. Ying et al., Physics and technology considerations for the deuterium–tritium fuel cycle and conditions for tritium fuel self sufficiency, Nucl. Fusion 61(1), 013001 (2021). https://doi.org/10.1088/1741-4326/abbf35

[6] S. Meschini, S. E. Ferry, R. Delaporte-Mathurin, and D. G. Whyte, Modeling and analysis of the tritium fuel cycle for ARC- and STEP-class D-T fusion power plants, Nucl. Fusion 63(12), 126005 (2023). https://doi.org/10.1088/1741-4326/acf3fc

[7] G. Federici, C. Bachmann, L. Barucca et al., Overview of the DEMO staged design approach in Europe, Nucl. Fusion 59(6), 066013 (2019). https://doi.org/10.1088/1741-4326/ab1178

[8] C. Day, K. Battes, B. Butler et al., The pre-concept design of the DEMO tritium, matter injection and vacuum systems, Fusion Eng. Des. 179, 113139 (2022). https://doi.org/10.1016/j.fusengdes.2022.113139

[9] T. Giegerich and C. Day, Conceptuation of a continuously working vacuum pump train for fusion power plants, Fusion Eng. Des. 88(9-10), 2206–2209 (2013). https://doi.org/10.1016/j.fusengdes.2013.05.019

[10] M. E. Sawan and M. A. Abdou, Physics and technology conditions for attaining tritium self-sufficiency for the DT fuel cycle, Fusion Eng. Des. 81(8-14), 1131–1144 (2006). https://doi.org/10.1016/j.fusengdes.2005.07.035

[11] S. Meschini, R. Delaporte-Mathurin, G. R. Tynan, and S. E. Ferry, Impact of trapping on tritium self-sufficiency and tritium inventories in fusion power plant fuel cycles, Nucl. Fusion 65(3), 036010 (2025). https://doi.org/10.1088/1741-4326/adacfa

[12] P.-C. A. Simon, C. T. Icenhour, G. Singh et al., MOOSE-based tritium migration analysis program, version 8 (TMAP8) for advanced open-source tritium transport and fuel cycle modeling, Fusion Eng. Des. 214, 114874 (2025). https://doi.org/10.1016/j.fusengdes.2025.114874

[13] Idaho National Laboratory, TMAP8: Fuel cycle benchmarking from Meschini et al. (2023), Technical documentation, accessed: Sep. 9, 2026. https://tmap8.inl.gov/examples/fuel_cycle_Meschini/index.html

[14] R. Delaporte-Mathurin, J. Dark, G. Ferrero, E. A. Hodille, V. Kulagin, and S. Meschini, FESTIM: An open-source code for hydrogen transport simulations, Int. J. Hydrog. Energy 63, 786–802 (2024). https://doi.org/10.1016/j.ijhydene.2024.03.184

[15] UK Atomic Energy Authority, Power balance models: A tokamak power balance model with Python API and CLI, Software repository, accessed: Sep. 9, 2026. https://github.com/ukaea/powerbalance

[16] G. Alva, Y. Lin, and G. Fang, An overview of thermal energy storage systems, Energy 144, 341–378 (2018). https://doi.org/10.1016/j.energy.2017.12.037

[17] N. A. Sepulveda, J. D. Jenkins, A. Edington, D. S. Mallapragada, and R. K. Lester, The design space for long-duration energy storage in decarbonized power systems, Nat. Energy 6(5), 506–516 (2021). https://doi.org/10.1038/s41560-021-00796-8

[18] N. Trosino, J. E. Parsons, R. Macdonald, C. Forsberg, and Y. Perez, Steady heat, flexible power: Flexibility by proxy in nuclear-thermal energy storage systems, MIT Center for Energy and Environmental Policy Research, Working Paper 2026-10, May 2026. https://ceepr.mit.edu/workingpaper/steady-heat-flexible-power-flexibility-by-proxy-in-nuclear-thermal-energy-storage-systems/

[19] B. Xu, J. Zhao, T. Zheng, E. Litvinov, and D. S. Kirschen, Factoring the cycle aging cost of batteries participating in electricity markets, IEEE Trans. Power Syst. 33(2), 2248–2259 (2018). https://doi.org/10.1109/tpwrs.2017.2733339

[20] A. Karpatne, G. Atluri, J. H. Faghmous et al., Theory-guided data science: A new paradigm for scientific discovery from data, IEEE Trans. Knowl. Data Eng. 29(10), 2318–2331 (2017). https://doi.org/10.1109/tkde.2017.2720168

[21] J. Willard, X. Jia, S. Xu, M. Steinbach, and V. Kumar, Integrating scientific knowledge with machine learning for engineering and environmental systems, ACM Comput. Surv. 55(4), 1–37 (2023). https://doi.org/10.1145/3514228

[22] L. Ljung, Analysis of recursive stochastic algorithms, IEEE Trans. Autom. Control 22(4), 551–575 (1977). https://doi.org/10.1109/tac.1977.1101561

[23] C. V. Rao, J. B. Rawlings, and D. Q. Mayne, Constrained state estimation for nonlinear discrete-time systems: stability and moving horizon approximations, IEEE Trans. Autom. Control 48(2), 246–258 (2003). https://doi.org/10.1109/tac.2002.808470

[24] N. J. Gordon, D. J. Salmond, and A. F. M. Smith, Novel approach to nonlinear/non-Gaussian Bayesian state estimation, IEE Proceedings F Radar and Signal Processing 140(2), 107–113 (1993). https://doi.org/10.1049/ip-f-2.1993.0015

[25] M. S. Arulampalam, S. Maskell, N. Gordon, and T. Clapp, A tutorial on particle filters for online nonlinear/non-Gaussian Bayesian tracking, IEEE Trans. Signal Process. 50(2), 174–188 (2002). https://doi.org/10.1109/78.978374

[26] C. Andrieu, A. Doucet, and R. Holenstein, Particle Markov chain Monte Carlo methods, Journal of the Royal Statistical Society Series B: Statistical Methodology 72(3), 269–342 (2010). https://doi.org/10.1111/j.1467-9868.2009.00736.x

[27] L. Hewing, K. P. Wabersich, M. Menner, and M. N. Zeilinger, Learning-based model predictive control: Toward safe learning in control, Annual Review of Control, Robotics, and Autonomous Systems 3(1), 269–296 (2020). https://doi.org/10.1146/annurev-control-090419-075625

[28] A. Mesbah, Stochastic model predictive control: An overview and perspectives for future research, IEEE Control Syst. 36(6), 30–44 (2016). https://doi.org/10.1109/mcs.2016.2602087

[29] D. Bertsimas and M. Sim, The price of robustness, Oper. Res. 52(1), 35–53 (2004). https://doi.org/10.1287/opre.1030.0065

[30] G. C. Calafiore and M. C. Campi, The scenario approach to robust control design, IEEE Trans. Autom. Control 51(5), 742–753 (2006). https://doi.org/10.1109/tac.2006.875041

[31] M. C. Campi and S. Garatti, The exact feasibility of randomized solutions of uncertain convex programs, SIAM J. Optim. 19(3), 1211–1230 (2008). https://doi.org/10.1137/07069821x

[32] M. C. Campi, S. Garatti, and F. A. Ramponi, A general scenario theory for nonconvex optimization and decision making, IEEE Trans. Autom. Control 63(12), 4067–4078 (2018). https://doi.org/10.1109/tac.2018.2808446

[33] D. Q. Mayne, J. B. Rawlings, C. V. Rao, and P. O. M. Scokaert, Constrained model predictive control: Stability and optimality, Automatica 36(6), 789–814 (2000). https://doi.org/10.1016/s0005-1098(99)00214-9

[34] D. Q. Mayne, Model predictive control: Recent developments and future promise, Automatica 50(12), 2967–2986 (2014). https://doi.org/10.1016/j.automatica.2014.10.128

[35] K. P. Wabersich and M. N. Zeilinger, A predictive safety filter for learning-based control of constrained nonlinear dynamical systems, Automatica 129, 109597 (2021). https://doi.org/10.1016/j.automatica.2021.109597

[36] R. T. Rockafellar and S. Uryasev, Optimization of conditional value-at-risk, The Journal of Risk 2(3), 21–41 (2000). https://doi.org/10.21314/jor.2000.038

[37] C. J. Clopper and E. S. Pearson, The use of confidence or fiducial limits illustrated in the case of the binomial, Biometrika 26(4), 404–413 (1934). https://doi.org/10.1093/biomet/26.4.404

[38] C. Barrows, E. Preston, A. Staid et al., The IEEE reliability test system: A proposed 2019 update, IEEE Trans. Power Syst. 35(1), 119–127 (2020). https://doi.org/10.1109/tpwrs.2019.2925557

[39] Grid Modernization Laboratory Consortium, RTS-GMLC: Reliability test system, Software and data repository, accessed: Sep. 9, 2026. https://github.com/GridMod/RTS-GMLC

[40] L. L. Lucas and M. P. Unterweger, Comprehensive review and critical evaluation of the half-life of tritium, Journal of Research of the National Institute of Standards and Technology 105(4), 541–549 (2000). https://doi.org/10.6028/jres.105.043

[41] B. Efron, Bootstrap methods: Another look at the jackknife, Ann. Stat. 7(1), 1–26 (1979). https://doi.org/10.1214/aos/1176344552

[42] C. Ruan, R. Guo, Z. Gong, J. Xu, W. Yang, and X. Chen, PRE-Mamba: A 4D State Space Model for Ultra-High-Frequent Event Camera Deraining, Proceedings of the IEEE/CVF International Conference on Computer Vision, 2025, pp. 9169–9180. https://doi.org/10.1109/ICCV51701.2025.00857

[43] P. Ma, Z. Zhou, C. Ruan, H. Wang, K. Li, Z. Gong, W. Ding, C. Gao, J. Xu, and X. Chen, EventPrune: Cascaded Event-Assisted Token Pruning for Efficient First-Person Dynamic Spatial Reasoning, Accepted for NeurIPS 2026. Preprint version: https://doi.org/10.48550/arXiv.2605.19506